Evidence of Rapid Flux Emergence Associated with the M 8.7 Flare on 2003 July 26

Haimin Wang[1,2], Jiong Qiu[2], Ju Jing[1,2], Thomas J. Spirock[1,2], Vasyl Yurchyshyn[1], Valantina Abramenko[1], Haisheng Ji[1] and Phillip R. Goode[1,2]

1. Big Bear Solar Observatory, New Jersey Institute of Technology 40386 North Shore Lane, Big Bear City, CA 92314-9672, USA

2. Center for Solar and Terrestrial Research, New Jersey Institute of Technology, Newark, NJ 07102

haimin@flare.njit.edu -- Version on October 31, 2003

ABSTRACT

In this paper, we present a detailed study of the M8.7 flare that occurred on July 26, 2002, using data from Big Bear Solar Observatory (BBSO), Ramaty High Energy Solar Spectroscopic Imager (RHESSI), Transition Region and Coronal Explorer (TRACE) and Solar and Heliospheric Observatory (SOHO). This flare has similar interesting properties to a number of flares that we studied previously, such as a rapid increase of magnetic flux in one polarity, and an increase in transverse fields and magnetic shear associated with the flare. However, this event had most comprehensive observations, in particular, the high resolution high cadence BBSO vector magnetograph observations. At the time of the flare, across the flare neutral line, there was a sudden emergence of magnetic flux at the rate of 10^{20} Mx/hr in both the longitudinal and transverse components. The emerging flux mostly occurred at the sites of the flare. It was very inclined and led to impulsively enhanced shear in the magnetic fields. We discuss these observations in the context of flux injection model.

Subject headings: Sun: activity – Sun: magnetic fields – Sun: flares

1. INTRODUCTION

Ever since the discovery of Coronal Mass Ejections (CMEs), various CME models have been developed (see Forbes 2001 for a review). These include the flux rope model (Low 1994; Forbes & Priest 1995; Amari et al. 2000; Chen 1989), the sheared arcade reconnection model

(e.g., Mikic et al. 1994, Magara et al. 1997, Choe et al. 2002), and the break-out model (e.g., Antiochos et al. 1999). Regardless of different configurations depicted by different models, it is believed that evolution of the magnetic fields at or below the photosphere, in the form of shear motion or flux emergence, results in the loss of equilibrium of the magnetic structure leading to the coronal mass ejection. For example, regarding the initiation of CMEs and the surface magnetic field activity, Chen et al. (1997) developed a theoretical model of CMEs and eruptive prominences based on the forces acting on toroidal magnetic flux ropes (Chen 1989). The predictions obtained from the model to date indicate that the poloidal flux injection process should produce subtle photospheric flows at less than the Alfven speed ($\ll$ 1 km/s), and changes (10-30%) in the tangential magnetic field over 30-60 min (Chen 1996, 2000), during the early phases of CME eruptions.

These changes of the photospheric magnetic fields should be studied observationally with respect to flares and CMEs. In terms of the magnetic flux change related with flares, several recent papers have provided some interesting observations. Kosovichev and Zharkova (2001) studied high resolution MDI magnetogram data for the 2000 July 14 "Bastille Day Flare" and found permanent decreases in magnetic fluxes. It was explained by the release of magnetic energy. Spirock et al. (2002) studied the X20 flare on April 2, 2001, the largest solar flare in the last few decades, and found that, after the flare, the magnetic flux of the leading polarity increased by approximately 6×10^{20} Mx, while there was no obvious change in the magnetic flux in the following polarity. Wang et al. (2002a) summarized the study of 6 X-class flares and found that unbalanced, rapid and permanent flux increase might be a common property of major solar flares. It now becomes clear that with high cadence (1 minute) and high resolution (1 to 2 arcsec) magnetic field observations, sudden flux changes associated with flares are observed to exist for at least some bigger events. Note that all the six events studied by Wang et al. (2002a) have flare associated CMEs, therefore, studying flare related magnetic field change will also shed light on the magnetic mechanism of CMEs.

In terms of the relationship between flares and the magnetic non-potentiality, it has been established, from the early studies of the relationship of solar flares to the morphology of an active region's magnetic field, that strong flares mostly occur near the neutral lines of the active region's vertical component of the magnetic field where there is a strong gradient in the magnetic field and where the horizontal component is strongly sheared. This shear in the horizontal component may experience substantial flare-related changes. Wang et al. (1994) determined that the magnetic shear of an active region may increase after the occurrence of an X-class flare. This result initially appears to be counter-intuitive as the magnetic shear is expected to decrease as the total magnetic energy of the active region decreases. Chen et al. (1994) studied more than 20 M-class flares and determined that there was essentially no apparent change in magnetic fields associated with the flares. The results

from studies conducted at the Marshall Space Flight Center (Ambastha et al., 1993; Hagyard et al, 1999) were inconclusive. The morphology of an active region's magnetic field may or may not change as the result of a solar flare and the magnetic shear in the active region may decrease, increase or remain unchanged. Recent studies of Wang et al. (2002a) also points to an increased shear for two events. However, the conclusions of these attempts have not been unambiguous because it is not easy to separate the tangential component contribution from other contributions, like seeing, and the decreased signal-noise ratio.

The event studied in this paper provides a very good opportunity to investigate the 3-d structure of magnetic structure associated with the flare: the event was close to disk center, the seeing was very good and stable and we had comprehensive coverage with BBSO vector magnetograph, RHESSI and TRACE observations.

2. OBSERVATIONS AND DATA REDUCTION

BBSO's Digital Vector Magnetograph (DVMG) system, has a much improved sensitivity and resolution compared to that of the old BBSO Videomagnetograph system. The hardware has been described in detail by Spirock et al. (2002). It consists of a 1/4 Å band pass filter, an SMD 1024 × 1024 12-bit CCD camera and three liquid crystals used as polarization analyzers. Each data set consists of four images: a 6103 Å filtergram (Stokes-I), a line-of-sight magnetogram (Stokes-V) and the transverse magnetogram (Stokes-U and -Q). We usually re-bin the camera to the 512 × 512 mode to increase the sensitivity of the magnetograms. After rebinning, the pixel resolution is about 0.6″. The line-of-sight magnetic sensitivity is approximately 2 Gauss while the transverse sensitivity is approximately 20 Gauss. The cadence for a complete set of Stokes images is typically 1 minute.

BBSO magnetograms cover a time range from 19UT to 00UT. In order to cover a longer time period and also have an independent confirmation of BBSO observations, we used high resolution, high cadence line-of-sight magnetograms from SOHO/MDI. MDI mainly obtains full-disk dopplergrams for the investigation of solar oscillations. In addition, MDI provides full disk longitudinal magnetograms with a cadence of 1 minute and an image scale of 2″ for some observing days (Scherrer et al., 1995).

In the past two and a half years, we have successfully installed and are continuously operating a high resolution global Hα network. The stations are at BBSO, Kanzelhohe Solar Observatory (KSO) in Austria, Catania Astrophysical Observatory (CAO) in Italy, Yunnan Observatory (YO) and Huairou Solar Observing Station (HSOS) in China. Nominally, each station obtains Hα image every minute with 1″ pixel resolution. The data are calibrated

using standard procedures from BBSO. The primary data to locate flare source in the current study are from full disk Hα data obtained at BBSO.

This event was covered by Transition Region And Corona Explorer (TRACE). It is a powerful instrument linking dynamic phenomena from the chromosphere through the transition region to the corona (Handy et al., 1999). TRACE usually covers a larger, but compatible field of view ($510''\times$ $510''$) to that of BBSO high resolution observations ($300''\times$ $300''$). For the event studied, TRACE covered different wavelengths before and after the flare (W.L, 1600Å before and 171Å after), as the flare triggered the corona observing mode. We concentrate our study on the post-flare loop structure.

Much of the energy released during a flare is used to accelerate electrons (emitting primarily X-rays) to very high energies and protons and other ions (emitting primarily gamma rays). The new approach of the RHESSI mission is to combine, for the first time, high-resolution imaging in hard X-rays and gamma rays with high-resolution spectroscopy, so that a detailed energy spectrum can be obtained at each point of the image (Lin et al., 2002). Such information advances our understanding of the fundamental high-energy processes at the core of the solar flare problem. RHESSI had post peak coverage on this flare. We were able to make maps from the available data.

According to the the CME list compiled by LASCO team, this event was accompanied by a fast Halo-CME that started to be observed by C2 at 22:30 UT, and its average speed was 800 km s^{-1}.

3. RESULTS

3.1. Measurements of Vector Magnetic Fields

Like our earlier studies, we first search for changes in the magnetic fields, which includes, line-of-sight magnetic fields (from measurement of circular polarization V) and transverse magnetic fields (from measurements of linear polarization Q and U). The amplitude of the transverse field is determined by:

$$B_T = C \times (Q^2 + U^2)^{\frac{1}{4}}$$

where C is a calibration constant, and the azimuthal angle is determined by:

$$\theta = \frac{1}{2}\arctan\left(\frac{U}{Q}\right)$$

In a previous paper (Wang, 1992), we defined the term "shear" as the product of the shear angle and the measured transverse field strength. This term was introduced to describe the magnetic shear in solar active regions. The shear angle is the angular difference between the transverse component of the model potential field and the measured transverse field. We introduced this definition of shear, instead of the pure shear angle defined by Hagyard et al. (1984, 1990), because (1) the strong transverse field regions contribute more significantly to the free magnetic energy of shear, and (2) the measurement errors in the azimuthal angles for strong field regions are significantly reduced. Since every point has a well-defined magnetic shear, two dimensional shear maps can be constructed. The time sequence of shear maps is compiled as shear movies in order to visualize evolution of the magnetic shear.

3.2. Flare-related Changes of Magnetic Fields

To demonstrate the morphology of the flare and relative position in the magnetograms, Figure 1 shows a BBSO line-of-sight magnetogram shortly before the flare, an Hα image overplotted by RHESSI contour in the energy range of 25 to 50 keV right after the flare peak, and a comparison of transverse magnetic fields before and after the flare. The red circle marks the area of a rapid increase of transverse magnetic field, which is co-spatial with the RHESSI loop-top source and connects two Hα ribbons.

Figure 2 plots the positive and negative line-of-sight magnetic flux, in absolute values, in the entire field of view (120 x 120 $''$) shown in Figure 1. The magnetograph data were from MDI, which covered a much longer period and are free of atmospheric seeing. The GOES X-ray light curve is overplotted to show the evolution of the flare emission. The figure shows that there is a continuous increase in both the positive and negative flux over 14 hrs, which is caused partially by gradual new flux emergence and partially by projection effects evolving with solar rotation, and can be approximated by a linear function of time, as shown in Figure 2. Apart from this linear evolution, we also find a rapid increase of the magnetic flux in the positive polarity at the time of the M8.7 flare. With the linear trend subtracted, the rapid rise of the positive flux amounts to 2×10^{20} Mx. The negative magnetic fields do not exhibit significant change relative to the linear trend. The flare-related magnetic flux change motivated us to study the higher resolution BBSO vector magnetograms in more detail, to pin-down the location and the nature of such a rapid change.

Figure 3 plots the temporal evolution of the magnetic flux and shear, using the vector

magnetic field observations by BBSO during 19 - 23 UT. Here we summarize the major results.

(1) The positive magnetic flux evolves in the same pattern as shown in MDI magnetograms. We can pin-point the area that contributed to the increase of the positive flux: at one of the flare foot points marked by the black box. Figure 3 shows that the positive flux integrated over the black box rapidly increased by 1.3×10^{20} Mx over about 1 hour, which confirms that most of the positive flux increase occurs at the site of the flare. The positive flux change rate is about 1×10^{20} Mx/hr at the maximum. The BBSO magnetograms also show slight negative flux increase in the white box. The observed trend of the negative flux is somehow different from MDI observations, because some long-term changes in MDI data are due to motions of fluxes in and out the field-of-view.

(2) The mean transverse field strength increased rapidly by 40 Gauss, or about 6% of the pre-flare fields, within an hour after the onset of the flare, and the area of the most obvious increase is between two footpoints as marked by the circle in Figure 1. Assuming that the emerging flux loop has a diameter of $20''$, approximately, the transverse flux increases by about 6.5×10^{20} Mx at the maximum, and the peak flux rising rate is larger than the longitudinal flux increase rate. This indicates an inclined (flat) flux emergence.

(3) The figure shows that the area before the flare have a moderate weighed mean magnetic shear of 66^o. Throughout the flare, the shear increases by 4 degree following the same pattern as the transverse field strength. The increase in the magnetic shear indicates that the magnetic fields become less potential after the flare.

(4) No change was found for the mean brightness (not shown in the figure), there is no evidence of sunspot appearance or disappearance (e.g., Wang et al. 2002b) associated with the flare. This also indicates that the changes in magnetic field are not due to change of line profile in the observation. Such a conclusion is further supported by the analysis of line profile associated with this flare using Imaging Vector Magnetograph at Haleakala, University of Hawaii (Ji et al., 2003).

These observations indicate rapid increase of both the magnetic flux and magnetic non-potentiality at the site of the flare, and the rate of the flare related flux change is of order 10^{20} Mx/hr in both the longitudinal and transverse flux. These further suggest that significant amount of sheared and inclined magnetic flux is impulsively injected into the site of the flare, agreeing with the second point in section 3.2.

3.3. Evolution of Flare and Filament

The Hα observations show two bright flare ribbons residing in magnetic fields of opposite polarities, as shown in Figure 1. These two ribbons are connected by the hard X-ray source seen by RHESSI. Hα observations reveal that both of the two ribbons exhibit expansion motion away from the magnetic neutral line during the impulsive phase. The expansion velocity profiles of the two ribbons are temporally correlated, both reaching the maximum at 21:05 UT, around the maximum of the flare. TRACE observed the flare in the coronal line during the decay phase. Figure 4 compares TRACE 171Å image with corresponding magnetogram. The two Hα ribbons are clearly linked by the TRACE loops. Figure 5 shows the evolution of the TRACE 171Å loops that keep rising over several hours after the flare maximum. Also, the alignment of these post-flare loops is not nearly vertical to but much inclined to the magnetic neutral line, suggesting sheared magnetic loops.

Observations of the expanding ribbons in Hα and rising post-flare EUV loops which connect the two ribbons suggest continuous formation of flare loops at rising altitudes, as would be described by the standard flare model (see Forbes & Acton 1996 and references therein). However, we also find that this flare is different from other events. The flare is not preceded by filament eruption. Although there is a filament right in the middle of the two ribbons, it remains still throughout the flare. Apparently the rising post-flare loops are formed above the filament so that the filament is not disturbed at all by the flare or CME. These observations suggest that this event does not comply with the flux rope model in a normal configuration (e. g., Low & Zhang 2002).

4. DISCUSSION

This event provided a remarkably clear example of rapid flux emergence, which shows an increase in the transverse fields in the middle of the loop and an increase in the longitudinal fields near the footpoints. The increase of the magnetic flux amounts to several times 10^{20} Mx in both the longitudinal and transverse components in a timescale of several tens of minutes. Therefore, the peak flux change rate is of order 10^{20} Mx/hr. Such changes are accompanied by the enhancement of magnetic non-potentiality as represented by the increase of the magnetic shear after the flare. We also note that although the flare is accompanied by a Halo-CME, the surface magnetic field changes took place mostly at the sites of the flares. This may suggest that the trigger of the mass ejection is rather localized. The observed enhancement of transverse field seem to match with the flux-rope injection model of Chen (1996) in the following aspects.

(1) A rapid increase of transverse fields following the flare, shows a rising, very inclined loop going through the photosphere. The increased magnetic shear is an indicator that the emerged loop is very much sheared.

(2) The field lines are very inclined as the TRACE post flare loops are very flat. This is also supported by the unbalanced flux increase. As we discussed in previous papers (e.g. Wang et al., 2002a), if the region is θ away from disk center, newly emerged flux will appear in one polarity –the polarity closer to the limb, provided that the inclination angle of the field line of the new flux is θ or smaller. For this event, $\theta = 20°$, so the inclination angle is about 20°, consistent with the appearance of TRACE loop.

(3) This rising loop is part of (or a triggering of) a big loop system in the corona, which lost equilibrium and expanded to form the flare and CME. Based on LASCO observations, this CME does not have the classic 3 components: front, cavity and filament. The filament in Hα in the neutral line did not erupt. Therefore, there is no evidence of opening of field line due to the eruption.

On the other hand, Chen's model is not implemented to depict the configuration of the flares, hence it remains unclear how to interpret the observed flare ribbon separation in the context of the flux-rope injection model.

The work is supported by NSF under grants ATM-0313591, ATM-0233931, and AST-9987366, NASA under grants NAG5-10910, NAG5-10212, and NAG5-12733, ONR under grant N00014-03-1-0093.

REFERENCES

Amari, T., Luciani, J.F., Mikic, Z., & Linker, J. 2000, ApJ, 529, L49

Ambastha, A., Hagyard, M. J., & West, E. A. 1993, Sol. Phys., 148, 277

Antiochos, S.K., DeVore, C.R., & Klimchuk, J.A. 1999, ApJ, 510, 485

Chen, J., 1989, Ap.J., 338, 453

Chen, J., 1996, JGR, 101, 27499

Chen, J. & Garren, F., 1993, GRL, 20,2319

Chen, J., Howard, R. A., Brueckner, G. E., Santoro, R., Krall, J., Paswaters, S. E., St. Cyr, O. C., Schwenn, R., Lamy, P. & Simnett, G. M., 1997, Ap. J. Letters, 490, L191

Chen, J., Santoro, R. A., Krall, J., Howard, R. A., Duffin, R., Moses, J. D., Brueckner, G. E., Darnell, J. A. & Burkepile, J. T., 2000, Ap.J., 533, 481

Chen, J., Wang, H., Zirin, H. & Ai, G. 1994, Sol. Phys., 154, 261

Choe, G. S. & Cheng, C. Z. 2002, Phys. Plasmas, 9, 2330

Forbes, T. G., 2001, EP&S, 53, 423

Forbes, T. G. & Priest, E. R., 1995, Ap.J. 446, 377

Forbes, T.G., & Acton, L. W. 1996, ApJ, 459, 330

Hagyard, M. J., Teuber, D., West, E. A. & Smith, J. B., 1984, Sol. Phys., 91, 115

Hagyard, M. J., Venkatakrishnan, P. & Smith, J. B., Jr., 1990, Ap.J.S., 73, 195

Hagyard, M.J., Start, B.A., and Venkatakrishnan, P., 1999, Sol. Phys., 184, 133

Handy, B. N. & TRACE Team, 1999, Sol. Phys., 187, 229

Ji, H., Wang, H., Li, J., Jiang, Y. & Goode, P.R., 2003, Ap.J. Letters, to be submitted

Kosovichev, A. G. & Zharkova, V.V., 2001, Ap. J. Letters, 550, L105

Lin, R. & RHESSI Team, 2002, Sol. Phys., 210, 3

Low, B. C. 1994, Plasma Phys., 1, 1684

Low, B. C. & Zhang, M. 2002, ApJ, 564, 53L

Magara, T., Shibata, K., & Yokoyama, T. 1997, ApJ, 487, 437

Mikic, Z. & Linker, J. A. 1994, ApJ, 430, 898

Scherrer, P. H., et al. 1995, Sol. Phys., 162, 129

Spircok, T. J., Yurchyshyn, V. & Wang, H., 2002, Ap. J., 572, 1072

Wang, H., 1992, Sol. Phys., 140, 85

Wang, H., Ewell, M. W., Zirin, H. & Ai, G. 1994, ApJ, 424, 436

Wang, H., Spirock, T.J., Qiu, J., Ji, H., Yurchyshyn, V., Moon, Y., Denker, C. & Goode, P.R., 2002a, Ap.J., 2002, 576, 497

Wang H., Ji, H., Schmahl E. J., Qiu, J., Liu, C. & Na, D., 2002b, Ap.J. Letters, 580, 177

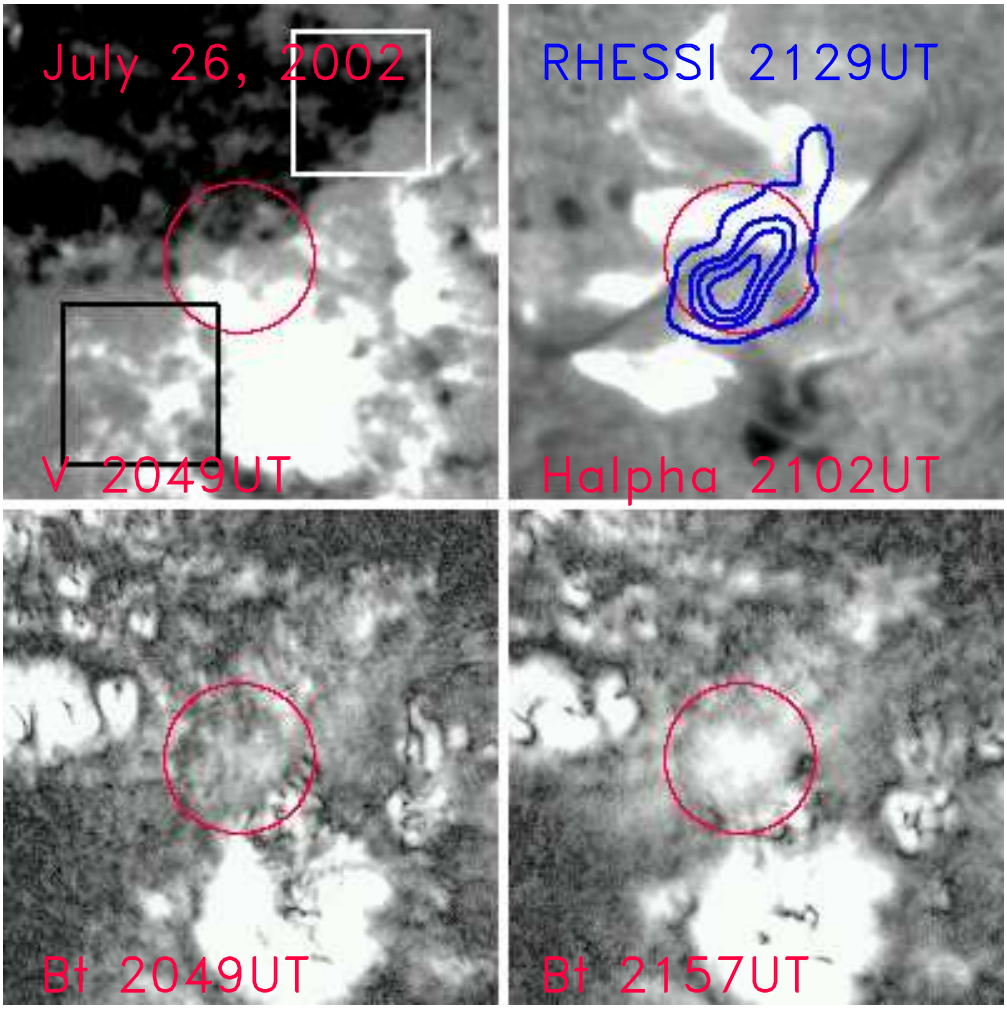

Fig. 1.— Top-left panel: line-of-sight magnetogram; Top-right panel: Hα flare ribbons and RHESSI hard X-ray image after the peak of the flare; Bottom Panels: comparison of transverse magnetic field before and after the flare. Squares and circle are areas of enhancement of longitudinal and transverse magnetic fields. The field of view is 120″ by 120″.

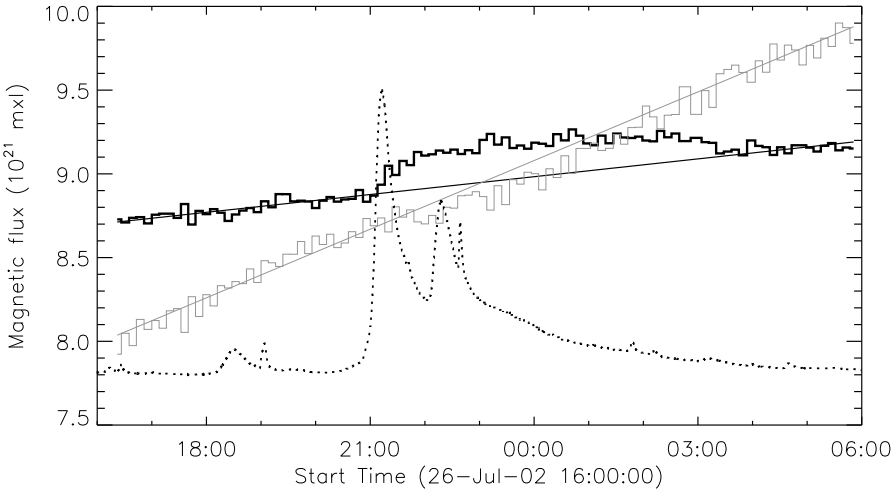

Fig. 2.— The evolution of magnetic flux over the entire field of view of Figure 1. The measurements are from MDI magnetograms. The darker solid lines are for positive flux and its linear fit; the lighter solid lines are for negative flux; the dotted line shows GOES soft X-ray flux.

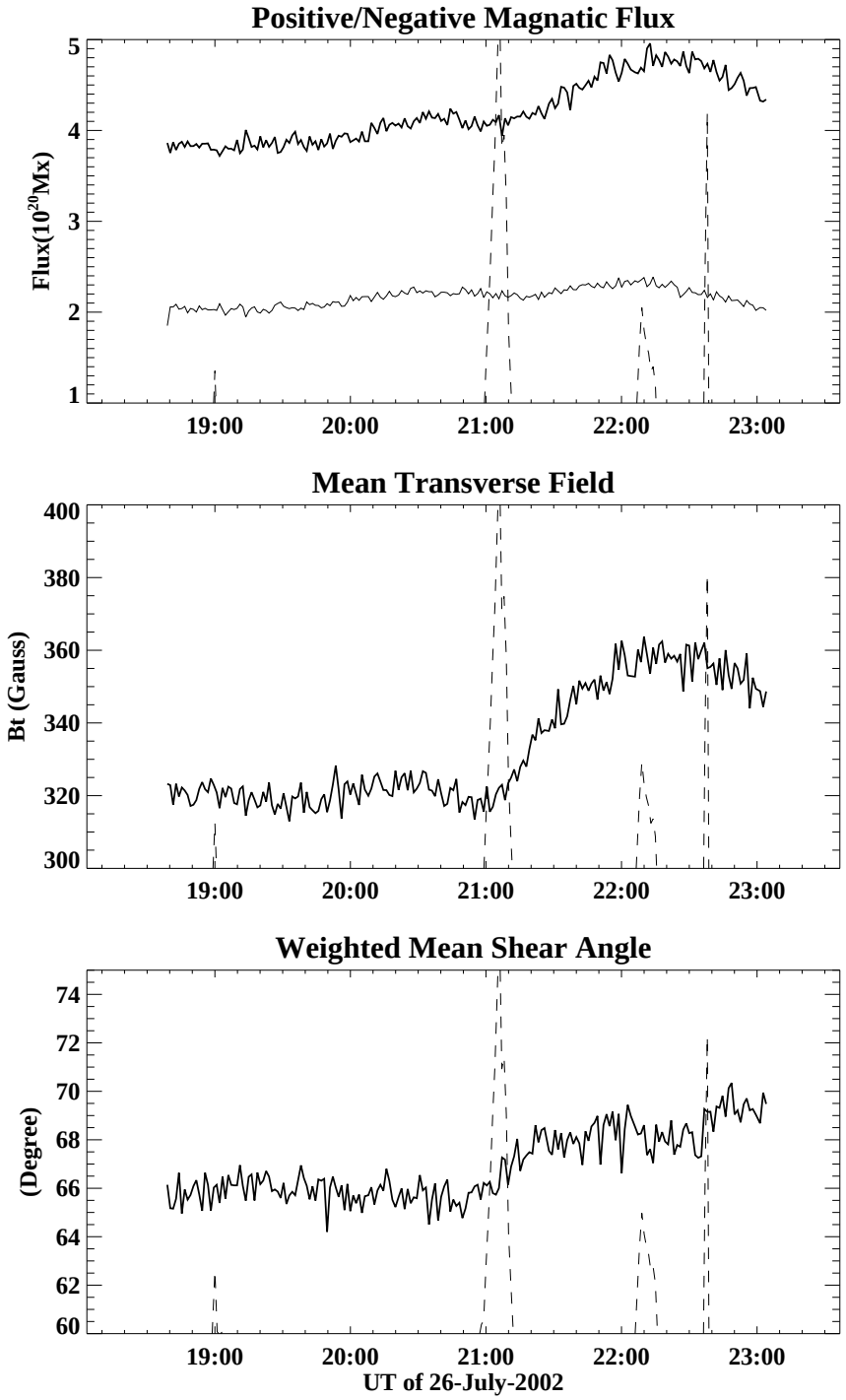

Fig. 3.— Time profiles of line-of-sight magnetic field, transverse field, and weighted mean shear angle. The dashed lines are derivatives of GOES X-ray flux.

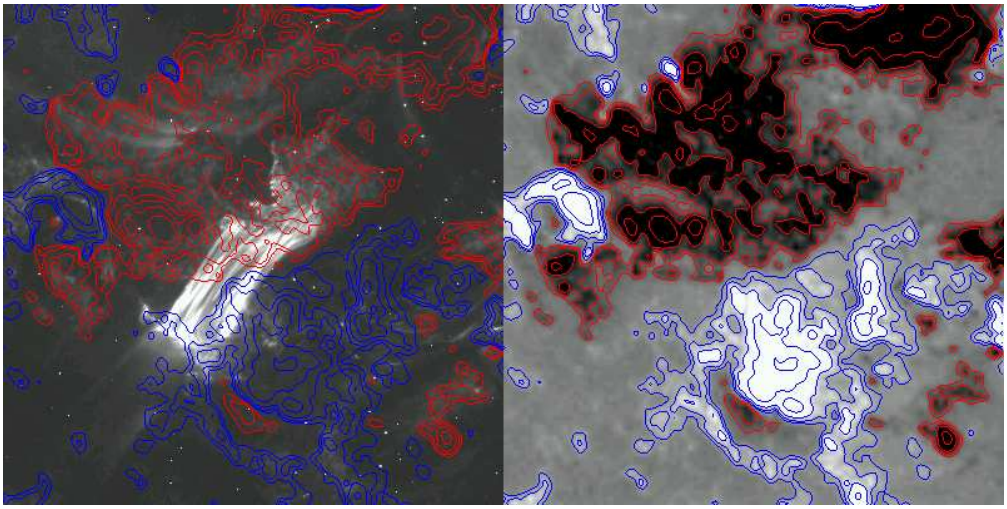

Fig. 4.— Left Panel: Comparison of contours of a magnetogram with TRACE 171Å image after the peak of the flare. Right Panel: Comparison of the gray-scale magntogram with its contours. The field of view is 200″ by 200″.

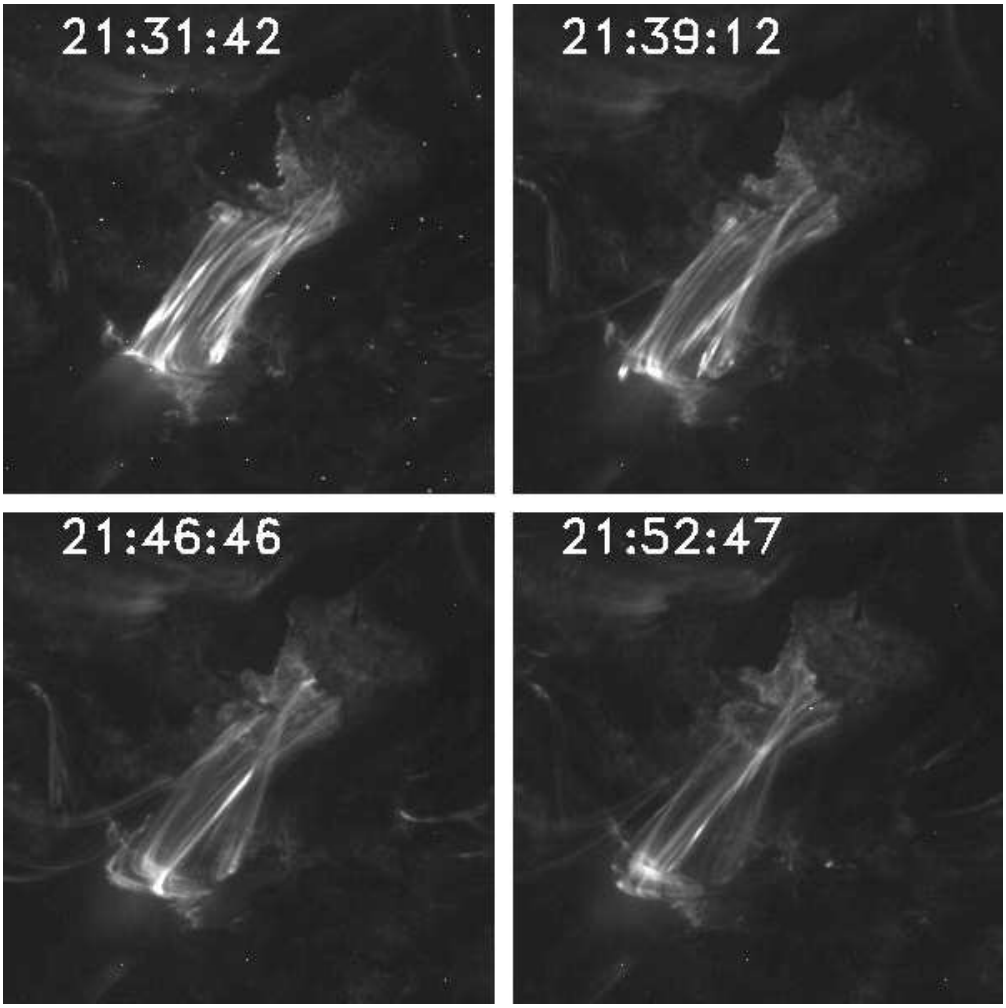

Fig. 5.— A sequence of TRACE images showing the slowly rising post-flare loop. The field of view is 200″ by 200″.